

A New Algorithm for Inverse Consistent Image Registration

Xiaojing Ye and Yunmei Chen

Department of Mathematics, University of Florida, Gainesville, FL 32611, USA

Abstract. This paper presents a novel variational model for inverse consistent deformable image registration. This model deforms the source and target image simultaneously, and aligns the deformed source and deformed target images in the way that the both transformations are inverse consistent. The model does not compute the inverse transforms explicitly, alternatively it finds two more deformation fields satisfying the invertibility constraints. Moreover, to improve the robustness of the model to noises and the choice of parameters, the dissimilarity measure is derived from the likelihood estimation of the residue image. The proposed model is formulated as an energy minimization problem, which involves the regularization for four deformation fields, the dissimilarity measure of the deformed source and deformed target images, and the invertibility constraints. The experimental results on clinical data indicate the efficiency of the proposed method, and improvements in robustness, accuracy and inverse consistency.

1 Introduction

Image registration is a very important subject and has been widely applied in medical research and clinic applications. The task of image registration is to find a transformation field that relates points in the source image to their corresponding points in the target image. Deformable image registration allows localized transformations, and is able to account for internal organ deformations. Therefore, it has been increasingly used in health care to assist diagnosis and treatments. In particular, deformable image registration has become a critical technique for image guided radiation therapy. It allows more precise tumor targeting and normal tissue preservation. A comprehensive review for image registration in radiation therapy can be found in [1].

A deformable image registration is called inverse consistent, if the correspondence between two images is invariant to the order of choice of source and target. More precisely, let S and T be the source and target images, and h and g be the forward and backward transformations, respectively, i.e. $S \circ h = T$ and $T \circ g = S$, then an inverse consistent registration satisfies $h \circ g = id$ and $g \circ h = id$, where id is the identity map. By applying an inverse consistent registration, measurements or segmentations from one image can be precisely transferred to the other. In imaging guided radiation therapy, the inverse consistent deformable registration technique provides the voxel-to-voxel mapping between the reference phase

and the test phase in four-dimensional (4D) radiotherapy [2]. This technique is referred to as "automatic re-contouring".

Inverse consistent deformable image registration has been an active subject of study in the literature. There have been a group of work that developed various of models in the context of large deformation by diffeomorphic metric mapping, e.g. [3,4,5,6]. The main idea of this method is modeling the forward and backward transformations as a one-parameter diffeomorphism group. Then, a geodesic path connecting two images is obtained by minimizing an energy functional symmetric to the forward and backward transformations.

Variational method is one of the popular approaches. This method minimizes the energy functional(s) symmetric to the forward and backward transforms, and in general, consists of three parts: regularization of deformation fields, dissimilarity measure on the target and deformed source image, and penalty of inverse inconsistency [7,8,9,10]. In [7], Christensen and Johnson proposed to minimize the following coupled energy functionals with respect to h and g alternatively:

$$\begin{cases} E(h) = E_1 + \rho \|h - g^{-1}\|_{L^2(\Omega)}^2 \\ E(g) = E_2 + \rho \|g - h^{-1}\|_{L^2(\Omega)}^2 \end{cases} \tag{1}$$

where $E_1 = \lambda E_s(S \circ h, T) + E_r(u)$, $E_2 = \lambda E_s(T \circ g, S) + E_r(v)$, $h(x) = x + u(x)$ and $g(x) = x + v(x)$. The dissimilarity E_s is defined as $E_s(S \circ h, T) = \|S \circ h - T\|_{L^2(\Omega)}^2$, and the regularity of deformation field u is defined as $E_r(u) = \|a \Delta u + b \nabla(\operatorname{div} u) - cu\|_{L^2(\Omega)}^2$ where $a, b, c > 0$ are constants. The last term in both energy functionals in (1) enforces the transforms h and g to be inverse to each other. This model solves a system of two evolution equations associated with their Euler-Lagrange (EL) equations iteratively, and gives considerably good results with parameters chosen carefully. However, it needs to compute the inverse mappings g^{-1} and h^{-1} explicitly in each iteration. This may cause accumulative numerical error in the estimation of inverses and is computationally intensive.

The variational models developed in [8] and [10] have the same framework as in [7] with different representations of E_s , E_r , and inverse consistent constraints. In both of work the terms $\|h \circ g(x) - x\|_{L^2(\Omega)}^2$ and $\|g \circ h(x) - x\|_{L^2(\Omega)}^2$ are used in the energy functional to enforce the inverse consistency. By using these terms the explicit computation of the inverse transforms of h and g can be avoided during the process of finding optimal forward and backward transformations. The similarity measure in [10] is the mutual information for multi-modal image registration. The $E_s(S \circ h, T)$ in [8] is $\|S \circ h - T\|_{L^2(\Omega)}^2 / \max |DT|$. The regularization term $E_r(u)$ in [10] is a function of Du , and that in [8] is a tensor based smoothing which is designed to prevent the transformation fields from being smoothed across the boundaries of features. In [11,12] the proposed models incorporated stochastic errors in the inverse consistent constraints for both forward and backward transformations.

In [13], Leow *et al.* proposed an approach that updates the forward and backward transformations simultaneously by a force that reduces the energies E_1 and E_2 in (1) and preserves the inverse consistency. However, it only takes linear order terms in the Taylor expression to approximate the inverse consistency and

hence the truncating errors can be accumulated and exaggerated during iterations. This results in large inverse consistent error, despite that it can produce a good matching quickly [14].

In this paper we propose a novel variational model to improve the accuracy, robustness and efficiency of inverse consistent deformable registration. The current framework of variational method finds the forward and backward transformations that deform a source image S to match a target image T and vice versa. In this work, we propose to deform S and T simultaneously, and the registration matches the deformed source and deformed target images. Since the disparity between deformed S and deformed T is smaller than that between deformed S and fixed T or deformed T and fixed S . Therefore, the deformation by the bidirectional simultaneous deformations is in general smaller than the deformation by unidirectional deformation that deforms S full way to T or T full way to S . Therefore, as shown in our experimental results deforming S and T simultaneously leads to a faster and better alignment than deforming S to the fixed T or vice versa. Let u and \tilde{u} represent the deformation fields such that $S(x + u)$ matches $T(x + \tilde{u})$. It is not difficult to verify that if u and \tilde{u} are invertible, then the registrations from S to T , and T to S are inverse consistent. To avoid the direct computation of the inverse transformations of $x + u(x)$ and $x + \tilde{u}(x)$, our model seeks for two additional deformation fields v , \tilde{v} such that $x + u(x)$ and $x + v(x)$ are inverse to each other, and the same for $x + \tilde{u}(x)$ and $x + \tilde{v}(x)$. Moreover, the registration process enforces certain regularity for these four deformation fields, and aligns the deformed S and deformed T . Then, the optimal inverse consistent transformations from S to T , and T to S can be obtained simply by appropriate compositions of these four transformations. Although the idea of deforming S and T simultaneously has been applied in the models where the forward and backward transformations as a one-parameter diffeomorphism group [5], our approach is different from the aspect that our model finds regularized invertible deformation fields rather than a one-parameter diffeomorphism group in [5], which brings expensive computational cost, and hence limits its application in clinic. Moreover, our model allows parallel computations for all the deformation fields to significantly reduce the computational time.

Furthermore, to improve the robustness of the model to noises and the choice of the parameter λ (1) in that balances the goodness of matching and smoothness of the deformation fields, we adopt the maximum likelihood estimation (MLE). This results in a self-adjustable weighting factor that makes the choice of λ more flexible, and also speeds up the convergence to the optimal deformation fields.

2 Proposed Method

For simplicity we suppose both the source image S and target image T are defined on $\Omega \subset \mathbb{R}^2$, and let $\|\cdot\|$ denote the L^2 norm hereafter.

In this paper, we propose to deform S and T simultaneously, and align the *deformed* S and *deformed* T . This means that ideally we pursuit for a pair of half-way transformations $\phi, \tilde{\phi} : \Omega \rightarrow \Omega$ such that $S \circ \phi = T \circ \tilde{\phi}$. To ensure

the transformations from S to T and T to S are inverse consistent, ϕ and $\tilde{\phi}$ are required to be invertible. To avoid direct computation of the inverses of ϕ and $\tilde{\phi}$ during iterations, we enforce the invertibility of ϕ and $\tilde{\phi}$ by seeking for $\psi, \tilde{\psi} : \Omega \rightarrow \Omega$, such that

$$\psi \circ \phi = id, \phi \circ \psi = id, \text{ and } \tilde{\psi} \circ \tilde{\phi} = id, \tilde{\phi} \circ \tilde{\psi} = id. \tag{2}$$

Then, once ψ and $\tilde{\psi}$ are obtained, we can construct the objective full-way transformations h and g that deform S to T and T to S using $h = \phi \circ \tilde{\psi}$ and $g = \tilde{\phi} \circ \psi$. From (2), it is clear that h and g also satisfy the inverse consistent constraints $h \circ g = g \circ h = id$. Let the functions u, \tilde{u}, v and \tilde{v} represent the corresponding deformation fields of the transformations $\phi, \tilde{\phi}, \psi$ and $\tilde{\psi}$, respectively, i.e.

$$\phi(x) = x + u(x), \tilde{\phi}(x) = x + \tilde{u}(x), \psi(x) = x + v(x), \tilde{\psi}(x) = x + \tilde{v}(x). \tag{3}$$

Then, the constraints (2) can be rewritten as

$$u + v(x + u) = v + u(x + v) = 0, \tilde{u} + \tilde{v}(x + \tilde{u}) = \tilde{v} + \tilde{u}(x + \tilde{v}) = 0. \tag{4}$$

Moreover, to improve the robustness of the algorithm, we use the negative log-likelihood of the residual image as a measure of mismatching. Consider pixel intensities of the residue image $W := S \circ \phi - T \circ \tilde{\phi}$ as independent samples drawn from a Gaussian distribution of zero mean and to be optimized variance σ^2 . Then we define the negative log-likelihood as the fitting term F :

$$F(u, \tilde{u}, \sigma) := \|S(x + u) - T(x + \tilde{u})\|^2 / 2\sigma^2 + |\Omega| \log \sigma. \tag{5}$$

The advantages of using MLE over the Sum of Squared Distance (SSD) as the fitting term will be shown later in this section and in the experimental results.

Now we propose our model as the following minimization problem:

$$\min_{u, \tilde{u}, v, \tilde{v}; \sigma} R(u, \tilde{u}, v, \tilde{v}) + \lambda F(u, \tilde{u}, \sigma), \text{ s.t. condition (4) holds,} \tag{6}$$

where R is the regularization of the deformation fields $(u, \tilde{u}, v, \tilde{v})$ defined by

$$R(u, \tilde{u}, v, \tilde{v}) := \|Du\|^2 + \|D\tilde{u}\|^2 + \|Dv\|^2 + \|D\tilde{v}\|^2. \tag{7}$$

By using (3), it is easy to see that the final full-way forward and backward deformation fields \bar{u} and \bar{v} can be obtained by

$$\bar{u} = \tilde{v} + u(x + \tilde{v}) \text{ and } \bar{v} = v + \tilde{u}(x + v), \tag{8}$$

respectively. Also, the inverse consistency of h and g can be preserved and $\bar{u} + \bar{v}(x + \bar{u}) = \bar{v} + \bar{u}(x + \bar{v}) = 0$, which can be derived from (4).

The term $F(u, \tilde{u}, \sigma)$ in (6) is from the negative log-likelihood of the residue image as in (5). Minimizing this term forces the mean intensity of the residue image to be zero, and allows it having a variance to accommodate certain variability. This makes the model more robust to noise and artifacts, and less sensitive to

the choice of the parameter λ than the model with the SSD. The parameter λ balances the smoothness of deformation fields and goodness of alignments, and affects the registration result greatly. In the proposed model, the ratio of the SSD of the residue image over the smoothing terms is $\lambda/2\sigma^2$ rather than a prescribed λ . Since σ is to be optimized, and from its EL equation σ is the standard deviation of the residue image., it updates the weight on the matching term during iterations. When the alignment gets better, the σ , i.e. the standard deviation of the residue as shown in (11), decreases, and hence the weight on the matching term automatically increases. This self-adjustable feature of the weight not only enhances the accuracy of alignment, but also makes the choice of λ flexible, and results in a fast convergence.

To solve problem (6), we convert the constraints to classical quadratic penalties in the energy functional, and obtain an unconstrained minimization problem

$$\min_{u, \tilde{u}, v, \tilde{v}; \sigma} R(u, \tilde{u}, v, \tilde{v}) + \lambda F(u, \tilde{u}, \sigma) + \mu (\mathcal{I}(u, v) + \mathcal{I}(\tilde{u}, \tilde{v})), \tag{9}$$

where $\mathcal{I}(u, v) = \mathcal{I}_v(u) + \mathcal{I}_u(v)$, $\mathcal{I}_v(u) = \|u + v(x + u)\|^2$ and $\mathcal{I}_u(v) = \|v + u(x + v)\|^2$. Similarly, we have $\mathcal{I}(\tilde{u}, \tilde{v})$. With sufficiently large μ , solving (9) gives an approximation to the solution of (6).

3 Numerical Scheme and Experimental Results

Since the compositions in the invertible constraints $\mathcal{I}_u(v)$ and $\mathcal{I}_v(u)$ bring in a difficulty to get explicit form of the EL equations for the deformation fields and their inverses, we solve the following two coupled minimization problems alternately instead of solving (9) directly:

$$\begin{cases} \min_{u, \tilde{u}} E_{v, \tilde{v}}(u, \tilde{u}) = \|Du\|^2 + \|D\tilde{u}\|^2 + \lambda F(u, \tilde{u}, \sigma) + \mu (\mathcal{I}_v(u) + \mathcal{I}_{\tilde{v}}(\tilde{u})) \\ \min_{v, \tilde{v}} E_{u, \tilde{u}}(v, \tilde{v}) = \|Dv\|^2 + \|D\tilde{v}\|^2 + \mu (\mathcal{I}_u(v) + \mathcal{I}_{\tilde{u}}(\tilde{v})). \end{cases} \tag{10}$$

whose EL equations can be computed in a straight forward manner. Also, the first variation of σ gives

$$\sigma = \|S(x + u) - T(x + \tilde{u})\|/|\Omega|^{1/2}. \tag{11}$$

It is important to point out that, in each iteration, the computations of $u, \tilde{u}, v, \tilde{v}$ can be carried out in parallel. To measure the accuracy of matching, we use the correlation coefficients (CC) between the target and deformed source images. Then, for fixed μ , our iterative process is terminated when the mean of $CC(S(x + \tilde{u}), T)$ and $CC(T(x + \tilde{v}), S)$ converges, and we can obtain $(u, \tilde{u}, v, \tilde{v})$ and hence \tilde{u} and \tilde{v} by (8). If the maximum inverse consistency error (ICE) δ_c , defined by

$$\delta_c = \max \{ |\tilde{u} + \tilde{v}(x + \tilde{u})|, |\tilde{v} + \tilde{u}(x + \tilde{v})| \mid x \in \Omega \}, \tag{12}$$

is large, one can gradually increase the parameter μ in (9) and use the previous $(u, \tilde{u}, v, \tilde{v})$ as a warm start. Then the whole computation can be stopped once

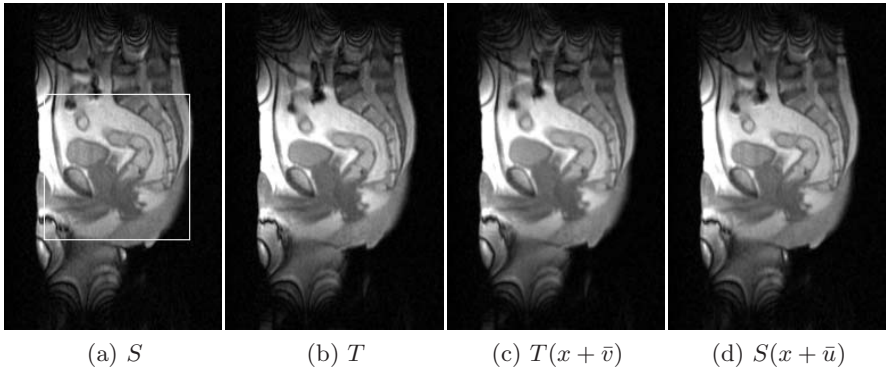


Fig. 1. Inverse consistent registration result by proposed model (9) on the prostate data, (c) and (d) are the deformed T and deformed S respectively

δ_c is less than a prescribed tolerance ϵ . In our experiments, we set $\epsilon = .5$, in which case the maximum ICE δ_c would be less than half of the grid size between two concatenate pixels/voxels and hence the invertibility is exactly satisfied with respect to the original resolution of the images.

We first test the accuracy of registration and auto re-contouring of the proposed algorithm on a clinical data set of 100 2D-prostate MR images. Each image, called a phase, is a 2D image of dimension 288×192 that focuses on prostate area. The first phase is used as a source image S , as shown in Fig 1a. The boundaries of the regions of interests (ROI) in S are delineated by contours and superimposed by medical experts, as enlarged and shown in Fig. 2d. The rest 99 phases are considered as target images. In this experiment we applied the proposed model (9) with parameters (λ, μ) set as $(.05, .2)$. For demonstration we only show the results using the 21st phase as T , as shown in Fig. 1b. The deformed T and deformed S are shown in Fig. 1c and 1d. The errors after the alignment $|S(x + \bar{u}) - T|$ and $|S - T(x + \bar{v})|$ in the squared area (as shown in Fig. 1a) are displayed in Fig. 2a and 2c, respectively. With comparison to the original error $|S - T|$ in Fig. 2b, we can see the errors after alignment are significantly reduced. This indicates that the proposed registration model (9) is highly accurate in matching two images. The final optimal forward and backward deformation fields \bar{u} and \bar{v} are displayed by applying them to a domain of regular grids, shown as Fig. 3a and 3b, respectively. Furthermore, to validate the well-preserved inverse consistency by model (9) we applied $\bar{u} + \bar{v}(x + \bar{u})$ on a domain of regular grids, and the resulting grids are plotted in Fig. 3c. The resulting grids by $\bar{v} + \bar{u}(x + \bar{v})$ has the same pattern so we omitted it here. From Fig. 3c, we can see that the resulting grids are the same as the original regular grids. This indicates that the inverse consistent constraints $\bar{u} + \bar{v}(x + \bar{u}) = \bar{v} + \bar{u}(x + \bar{v}) = 0$ are almost exactly satisfied. We also computed the maximum ICE δ_c using \bar{u}, \bar{v} and (12), which is .46 of a pixel. The mean ICE $(\|\bar{u} + \bar{v}(x + \bar{u})\| + \|\bar{v} + \bar{u}(x + \bar{v})\|) / 2|\Omega|$

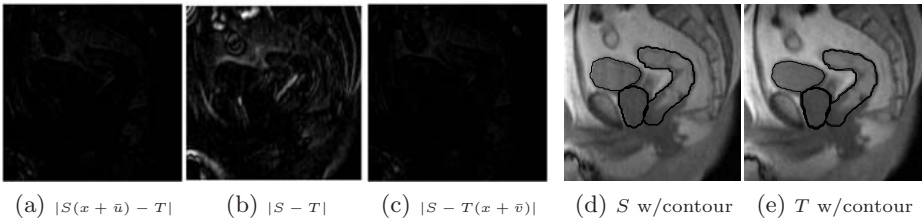


Fig. 2. Results of model (9) applied to S and T in the squared area shown in Fig. 1a. Contours in (e) are obtained by deforming the contours in (d) using \bar{u} .

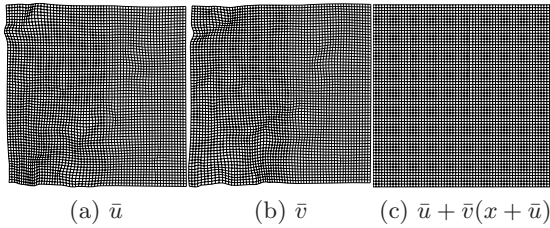


Fig. 3. Deformation fields applied to regular grids

versus the number of iterations are plotted on the right of Fig. 3, which shows the inverse consistency is preserved in the registration.

One of the applications of this algorithm is auto re-contouring, that deforms the expert’s contours from a planning image to new images during the course of radiation therapy. In this experiment, we had expert’s contours superimposed in the square area of the source image S as shown in Fig. 2d. Then by applying the deformation field \bar{u} on these contours we get the deformed contours on the target image T as shown in Fig. 2e. The accuracy in auto re-contouring is evident.

The second experiment was aimed to test the effectiveness of the proposed model (9) in registering 3D images. We applied this model to a pair of 3D brain MR images of dimension $128 \times 128 \times 73$ taken from two different subjects. The parameters (λ, μ) were set to be $(.05, .1)$. The registration is performed in 3D, but for demonstration, we only show the corresponding sagittal (xy plane with $z = 53$), coronal (yz plane with $x = 47$) and axial (zx plane with $y = 97$) slices as in the top, middle and bottom rows of Fig. 4, where the columns in Fig. 4a and 4b show the corresponding slices of S and T , respectively, and columns in Fig. 4c and 4d deformed T and deformed S , i.e. $\bar{T} := T(x + \bar{v})$ and $\bar{S} := S(x + \bar{u})$, respectively. Columns in Fig. 4e, 4f and 4g are $|S - T|$, $|S(x + \bar{u}) - T|$ and $|S - T(x + \bar{v})|$, respectively. The initial $CC(S, T) = .736$, and $CC(\bar{S}, T)$ and $CC(\bar{T}, S)$ reach .946 and .941 after 200 iterations, and the mean of inverse consistency errors is .027. The results show the high accuracy and well preserved inverse consistency obtained by using proposed model (9).

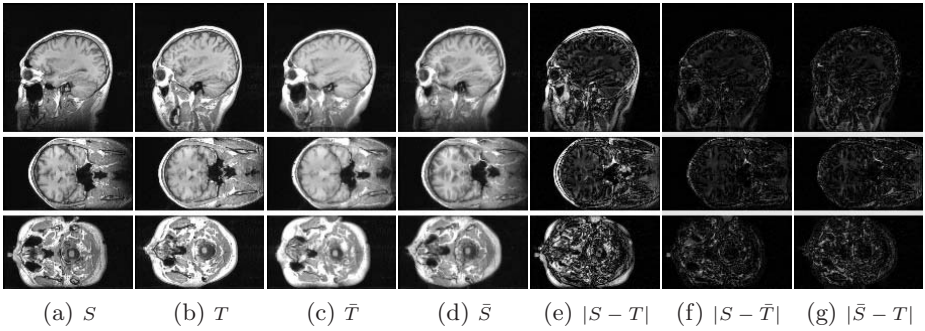


Fig. 4. Registration result of proposed model (9) applied to 3D brain MR image. The results of slices $z = 53$, $x = 47$ and $y = 97$ are plotted on the top, middle and bottom rows, respectively. Here $\bar{T} := T(x + \bar{v})$ and $\bar{S} := S(x + \bar{u})$.

The third experiment was aimed to compare the efficiency of model (9) with the conventional full-way inverse consistent deformable registration model:

$$\min_{u,v,\sigma_u,\sigma_v} \|Du\|^2 + \|Dv\|^2 + \lambda J(u, v, \sigma_u, \sigma_v) + \mu (\mathcal{I}_v(u) + \mathcal{I}_u(v)) \quad (13)$$

where u and v are forward and backward deformation fields, respectively, and the term J is defined by $J(u, v, \sigma_u, \sigma_v) = \|S(x + u) - T\|^2/2\sigma_u^2 + \|T(x + v) - S\|^2/2\sigma_v^2 + |\Omega| \log \sigma_u \sigma_v$. The comparison was made on the efficiency and accuracy of matching, as well as the ability of preserving inverse consistency. In this experiment we applied models (13) and (9) to the images in the first experiment shown in Fig. 1 with parameters (λ, μ) in both models set to be $(.05, .2)$. On the left Fig. 5, we plotted the CC obtained by model (13) and proposed model (9) at each iteration. It can be observed that the CC obtained by model (9) is higher and increases faster than that by model (13). This demonstrates that proposed model (9) is more efficient than the conventional full-way model. The reason is that the disparity between both deformed S and deformed T must be smaller than that between deformed S and fixed T or deformed T and fixed S . When S and T are deformed simultaneously, the two deformation fields u and \tilde{u} are not necessarily to be large even if the underlying deformation field is large, which usually makes it difficult for the full-way based registration model to reach a satisfactory alignment in reasonable time.

The last experiment was aimed to test the robustness of the model to noises and the choice of the parameter λ with the use of MLE based disparity measure (5). The images S and T in Fig. 1 with additive Gaussian noises (using Matlab function `imnoise` with standard deviation being 3% of largest intensity value of S) were used in this experiment. The CC between S and T before registration was $CC(S, T) = .901$. We applied model (9) to the noisy data with σ updated using its EL equation (11), as well as σ fixed to be 1, which is equivalent to using SSD as similarity measure. We proceeded the registration with various values of λ , but kept other parameters unchanged. Then the numbers of iterations (Iter) for convergence and the final CC were recorded and shown in Table 1. One can

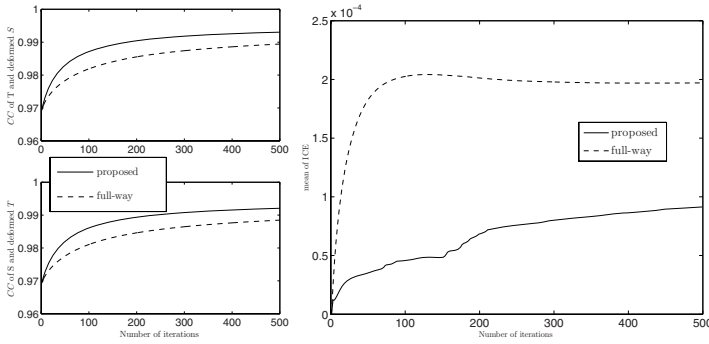


Fig. 5. Left: CC in each iteration obtained by full-way model (13) and proposed model (9). Right: Mean of inverse consistent errors (ICE) of the final deformation fields obtained by using full-way model (13) and proposed model (9).

see that while λ decreases, the accuracy of model (9) using fixed σ reduces as the final CC become much smaller, and it also takes significantly longer time for the algorithm to converge. On the other hand, with σ being updated (whose computational cost is extremely cheap) model (9) can obtain good matching in much less iterations for a large range of λ . This shows that model with MLE fitting is much less sensitive to noise and the choice of λ , and can achieve fast and accurate results compared with the model using SSD as the disparity measure.

Table 1. Number of iterations used for convergence and the final CC obtained by proposed model (9) with σ updated/fixed. For a large range of λ , updating σ in each iteration consistently leads to faster convergence and higher accuracy.

λ	Update σ		Fix σ	
	CC	Iter	CC	Iter
1e2	.962	48	.955	89
1e1	.962	97	.946	420
1e0	.960	356	.933	1762

4 Conclusion

In this work, we proposed a novel registration model that is featured at finding two invertible transformations that deform the source and target image simultaneously, and the registration process aligns both of the deformed source and deformed target images. From the theoretical analysis and experimental results, one can see the proposed model produces a fast convergence of the objective deformation field as well as provides a better correspondence for the ROIs in source and target images. This makes the auto re-contouring results with data involved in the course of radiation therapy much more accurate and efficient.

References

1. Kessler, M.L.: Image registration and data fusion in radiation therapy. *Br. J. Radiol.* 79, 99–108 (2006)
2. Lu, W., Olivera, G.H., Chen, Q., Chen, M., Ruchala, K.: Automatic re-contouring in 4d radiotherapy. *Phys. Med. Biol.* 51, 1077–1099 (2006)
3. He, J.C., Christensen, G.E.: Large deformation inverse consistent elastic image registration. In: Taylor, C.J., Noble, J.A. (eds.) *IPMI 2003*. LNCS, vol. 2732, pp. 438–449. Springer, Heidelberg (2003)
4. Joshiand, S., Davis, B., Jomier, M., Gerig, G.: Unbiased diffeomorphic atlas construction for computational anatomy. *Neuroimag. Suppl.* 23, 151–160 (2004)
5. Avants, B.B., Grossman, M., Gee, J.C.: Symmetric diffeomorphic image registration: Evaluating automated labeling of elderly and neurodegenerative cortex and frontal lobe. In: Pluim, J.P.W., Likar, B., Gerritsen, F.A. (eds.) *WBIR 2006*. LNCS, vol. 4057, pp. 50–57. Springer, Heidelberg (2006)
6. Beg, M.F., Khan, A.: Symmetric data attachment terms for large deformation image registration. *IEEE Trans. Med. Imag.* 26, 1179–1189 (2007)
7. Christensen, G.E., Johnson, H.J.: Consistent image registration. *IEEE Trans. Med. Imag.* 20, 721–735 (2001)
8. Alvarez, L., Deriche, R., Papadopoulos, T., Sanchez, J.: Symmetrical dense optical flow estimation with occlusions detection. In: *Euro. Conf. Comput. Vision*, pp. 721–735 (2002)
9. Rogelj, P., Kovacic, S.: Symmetric image registration. *Med. Imag. Anal.* 10, 484–494 (2006)
10. Zhang, Z., Jiang, Y., Tsui, H.: Consistent multi-modal non-rigid registration based on a variational approach. *Pattern Recognit. Lett.* 27, 715–725 (2006)
11. Yeung, S., Shi, P.: Stochastic inverse consistency in medical image registration. In: *International Conference on Medical Image Computing and Computer-Assisted Intervention*, vol. 8, pp. 188–196 (2005)
12. Yeung, S.K., Tang, C.K., Shi, P., Pluim, J.P., Viergever, M.A., Chung, A.C., Shen, H.C.: Enforcing stochastic inverse consistency in non-rigid image registration and matching. In: *IEEE Conf. CVPR*, pp. 1–8 (2008)
13. Leow, A., Huang, S., Geng, A., Becker, J., Davis, S., Toga, A., Thompson, P.: Inverse consistent mapping in 3d deformable image registration: its construction and statistical properties. In: *Proc. Inf. Process. Med. Imag.*, pp. 493–503 (2005)
14. Zeng, Q., Chen, Y.: Accurate inverse consistent non-rigid image registration and its application on automatic re-contouring. In: *Int. Symp. Bioinfo. Res. App.*, pp. 293–304 (2008)